Resolving Fast Gas Transients with Metal Oxide Sensors

Damien Drix* and Michael Schmuker

ACCESS | 📊 Metrics & More | 📰 Article Recommendations | 🆘 Supporting Information

ABSTRACT: Electronic olfaction can help detect and localize harmful gases and pollutants, but the turbulence of the natural environment presents a particular challenge: odor encounters are intermittent, and an effective electronic nose must therefore be able to resolve short odor pulses. The slow responses of the widely used metal oxide (MOX) gas sensors complicate the task. Here, we combine high-resolution data acquisition with a processing method based on Kalman filtering and absolute-deadband sampling to extract fast onset events. We find that our system can resolve the onset time of odor encounters with enough precision for source direction estimation with a pair of MOX sensors in a stereo-osmic configuration.

Electronic olfaction has potential in many areas such as industrial and environmental monitoring and safety, where it can help detect and localize harmful gases or pollutants. However, in natural environments, odors are dispersed by turbulent plumes and encounters are intermittent.[1] The temporal statistics of these odor pulses (hereafter also called *bouts*) contain information about source location.[2] An effective electronic nose thus needs to resolve both short pulses and pulses in rapid succession. Metal oxide (MOX) gas sensors are widely used, but have impulse response durations on the order of tens to hundreds of seconds,[3] and are therefore often thought to be of limited utility in turbulent environments.

However, a large part of the impulse response is due to a slow sensor recovery phase, on the order of 100 s, in which the sensor conductance slowly returns to the baseline while the initial reaction of the volatiles with the sensor electrode is reversed.[4] The onset of the response itself is near-instantaneous and can be detected after fractions of a second. Therefore, repeated short-duration bouts could be detectable with the help of specific physical mitigation (for instance, sensor purging[5] or pulsed heating[6]) or through signal processing that separates the initial binding from the recovery phase.

Here, we built a multichannel MOX sensor electronic nose with high bit depth and sampling rate to investigate how much can be achieved through signal processing alone. We developed a signal processing method based on a Kalman filter and absolute deadband sampling to isolate successive bouts and encode their onset time. We demonstrate the system's ability to resolve onset times and repeated bouts in a stereo-enose setup that infers the direction of a puff of odorant from stereo delays.

RESULTS

Data Acquisition. Our gas sensor boards consist of four metal oxide (MOX) sensors and a high-resolution analog-to-digital converter (ADC). We use four sensors manufactured by Figaro Inc. (Osaka, Japan): TGS2600, TGS2602, TGS2610, and TGS2620, to cover a wide range of target gases. The ADC (ADS122C04, Texas Instruments) offers 24 bits of resolution and can sample all four sensor channels at a frequency of up to 200 Hz. As MOX sensors are affected by ambient temperature and humidity, the boards can also host an optional 16-bit digital temperature and humidity sensor (SHT31-DIS, Sensirion).

An I2C bus operating at 800 kHz connects the boards to a microcontroller (Teensy 4.0, PJRC.COM) that reads out the data and transmits it to the host computer via USB (Figure 1). The system is set up so that the microcontroller can handle multiple sensors in parallel, for instance, left and right electronic noses in a stereoconfiguration.

The gas sensors are connected to the ADC in the voltage divider configuration that is standard for this type of sensor,[7] with the sensing element RS in series with a load resistor RL (Figure 1). This configuration works well with the chosen ADC as it allows a ratiometric measurement relative to the power supply, free from common-mode noise. On the other hand, its sensitivity degrades as RS deviates from RL, which normally requires an adjustable RL calibrated for a specific sensor at a given temperature and expected gas concentration.
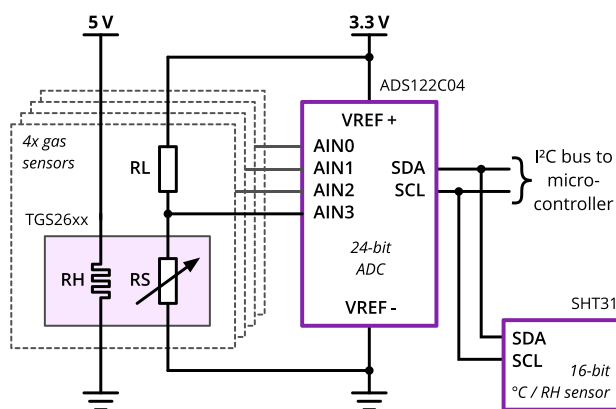
Figure 1. Simplified schematic of the sensor boards. The ADC on each sensor board measures the voltage across the MOX sensing elements RS. A separate 5 V supply powers the heating elements RH. The sensor board communicates via I2C with a Cortex-M7 microcontroller that transmits the data to the host computer.

Here, we make use of the ADC's high resolution and variable input gain instead, which lets us pick a fixed load resistor $RL = 68$ kΩ and still maintain a good sensitivity through a large range of concentrations and ambient conditions (Figure 2).
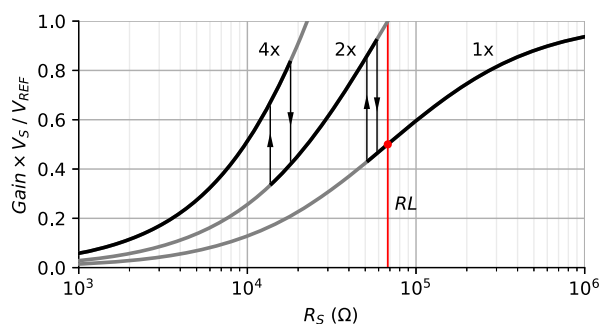

Figure 2. Automatic input gain selection maintains sensitivity over a large input range. ADC measurement for a varying sensor resistance RS at gain settings 1×, 2×, and 4×. RS follows an approximate power law with respect to gas concentration; thus, it makes sense to use a logarithmic scale, where the slope of the measurement function indicates the sensitivity to a relative change (e.g., ±1% in gas ppm). Thin arrows indicate the thresholds at which we increase or decrease the input gain to avoid the regions of lower sensitivity. The red line indicates the load resistance RL for reference.

The ADC measures a ratio $x = \frac{V_S}{V_S + V_L}$, where V_S and V_L are the voltages across RS and RL, respectively. From this, we compute the relative conductance g_{rel} of each sensor relative to its load resistor

$$g_{rel} = \frac{g_S}{g_L} = \frac{V_L}{V_S} = \frac{1}{x} - 1$$

Then, we divide by the baseline values at the start of each recording to get the normalized sensor conductance g at time t

$$g(t) = \frac{g_{rel}(t)}{g_{rel}(0)}$$

The purpose of the normalization is to use the same parameters for processing multiple sensors with different characteristics. It is not fundamentally required, since none of

the algorithms assume a specific or constant baseline value for g.

In preliminary work, we had found the quantization noise from 10-bit ADCs to be not insignificant compared to the signals of interest, complicating downstream processing. The 24-bit ADC solves this problem, and its good noise performance lets us resolve very low amplitude fluctuations (see Supporting Information Figure S-1).

Experimental Setup. We deliver puffs of isopropyl alcohol (IPA) to the sensors by means of a soft plastic bottle (NeilMed Inc., USA) squeezed by a servomotor to force vapors out of the nozzle (Figure 3). This creates a sharp puff that we could observe up to 50 cm from the nozzle in a quiet atmosphere.

We record simultaneously from two identical boards placed along the direction of travel of the puff. This yields four pairs of stereo channels (S0 to S3), one for each MOX sensor type. We aim the stimuli slightly downward onto a flat surface and position the top of the MOX sensors flush with that surface to reduce turbulence caused by the sensors themselves, which might otherwise disrupt the narrow odor plume before it reaches sensors on the far side. We record one data set with the stimulus traveling in the left-to-right direction, and then move the bottle to the other side and record another data set for the right-to-left direction.

Post-Processing. MOX sensors respond to puff of odorants with a fast rising phase, followed by a slower decay back to baseline (Figure 4A). This slow decay can mask fast transients, for instance, when two bouts occur close together in time (see, e.g., Figure 5A). The goal of post-processing is to isolate the onset of the rising phase, thus providing the ability to resolve short odor pulses. Various solutions have been explored in previous work, such as taking the second derivative or deconvolution based on an estimate of the sensor's impulse response function,[2] blind deconvolution,[8] and band-pass filters.[9]

Here, we use a constant-acceleration Kalman filter to compute a denoised estimate of the second derivative of the signal. The second derivative peaks at the onset of each puff (Figure 4A). However, it also has a second, smaller positive peak when the relaxation slows down, since that registers as a positive acceleration (Figure 4B). As this could cause spurious bout detections (it is very small compared to the onset response, but still 5 times larger than our bout detection threshold), we modify the filter to suppress the second peak. We do this by incorporating an exponential decay term into the system equations for the first derivative v, thus removing the expected relaxation from the residual second derivative a

$$g(t + dt) = g(t) + v(t)\, dt + \left(a(t) - \frac{v(t)}{\tau}\right)\frac{dt^2}{2}$$

$$v(t + dt) = v(t) + \left(a(t) - \frac{v(t)}{\tau}\right) dt$$

$$a(t + dt) = a(t)$$

The parameter τ sets the time constant of the decay term. We estimate it empirically for each sensor type, selecting the highest value which still suppresses the second peak. We also define a variable $o = \int a(t)\, dt$, which we call *bout velocity*. Being the integral of the residual second derivative a, this variable is essentially a first derivative of the signal, like v, but with the second peak removed.
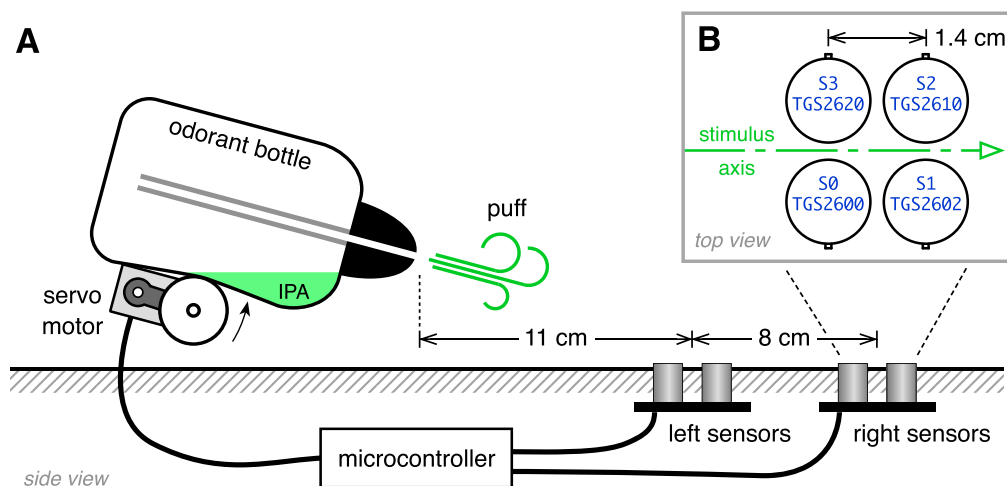
Figure 3. Automated setup delivers puffs of odorant toward stereo sensor boards. A: Side view of the system in its left-to-right configuration. B, inset: top view of a sensor board showing the position of the four sensors in relation to the stimulus axis.
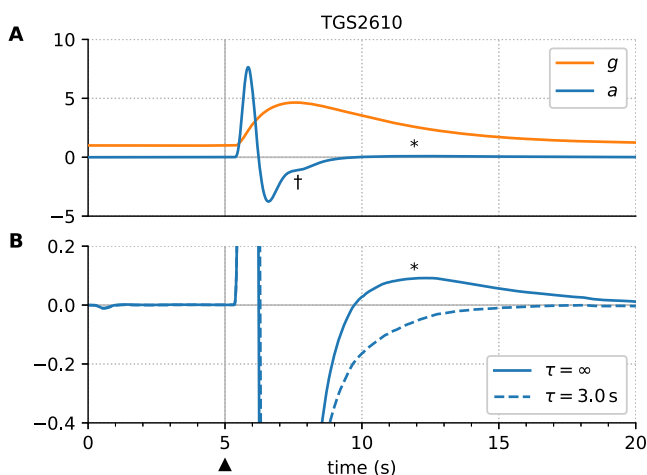

Figure 4. Kalman filtering recovers the onset of odorant bouts. The arrowhead (▲) marks the time when the odorant bottle is squeezed. A. Conductance g and its second derivative a estimated by the Kalman filter. B. Zooming in shows the effect of the filter parameter τ on the late-phase response. The second peak (*) is effectively removed with $\tau = 3$ s without affecting the early response. The feature marked † is unrelated and probably caused by a transient disturbance of the sensor.

Event-Based Onset Encoding. For the purpose of bout detection, it is the time of the odorant onset that matters, more than the precise time course of the sensor conductance during and after the bout. Therefore, it makes sense to transform the continuous filter output into an event-based representation that only transmits information during periods of increasing conductance.

We employ an event-based encoding related to delta modulation that has been variously called *deadband sampling*[10] or *send-on-delta*,[11] and is also used in the DVS camera.[12]

If the variable's value at a time t is $z(t)$ and the time of the last event is t_{prev}, then a new event is emitted whenever the difference exceeds a certain threshold $\theta = 0.02$

$$|z(t) - z(t_{prev})| > \theta$$

This form of absolute deadband sampling yields a stream of events with an instantaneous rate $f(t) \propto \left|\frac{d}{dt}z(t)\right|$, as the

algorithm differentiates. The sign of the difference indicates whether the variable increased (ON events) or decreased (OFF events). We discard all OFF events as these do not correspond to the onset of a bout.

This event-based encoding can be applied to the sensor conductance ($z = g$, for an event rate f proportional to v), as well as to the bout velocity variable ($z = o$, for an event rate f proportional to the filter output a). We find that when applied to the filter output, it produces well-separated bursts of events for two bouts separated by 5 s, a much shorter delay than the recovery phase of the sensor conductance (Figure 5B,D). On the other hand, events generated from the sensor conductance are prone to merging into a single burst when bouts follow each other closely (Figure 5A).

Direction Detection in Stereo-Osmic Configuration. We apply this event-based encoding to the data obtained from our recording setup in stereo-osmic configuration (Figure 3). As the stimulus travels over the sensors, the left and right sensor boards will detect its onset at slightly different times, with the delay between left and right boards depending on the speed and direction of the puff. We extract the time of the first event on each channel, and then compute the time differences between the left and right sensors (Figure 6). We find that the sign of that time difference encodes the direction of the stimulus unambiguously, despite some variance due to turbulent flow. A slight systematic offset is apparent between channels. We have observed a similar effect when the axis of the puff deviates from the center line; thus, the offset may be due to lateral flow, although mismatched sensor characteristics may also play a role.

■ DISCUSSION

We show that off-the-shelf metal oxide sensors can resolve relative onset delays in the subsecond range using a Kalman filter to extract bout onset times. This software approach could be combined with hardware measures[5,6] to increase the temporal resolution of the data even further.

The proposed method is inherently robust to baseline drift, a common issue with MOX sensors where their conductance at a certain odorant concentration will vary over the lifetime of the sensor and across the slower changes in ambient temperature and humidity.
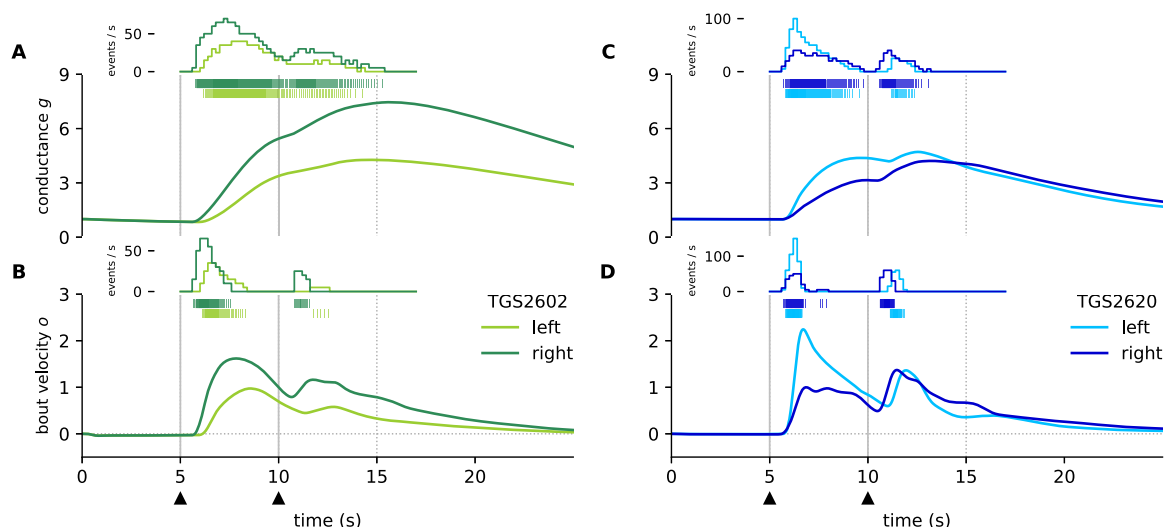
Figure 5. Events generated from the bout velocity variable isolate the onset of each bout. Responses of two sensor pairs during the same trial with two puffs of odorant (▲) at a 5 s interval in the right-to-left direction. A,B. Conductance g and bout velocity o estimated by the Kalman filter for the TGS2602 sensors (left and right), together with the resulting events (thin vertical lines) and event rate (time histogram). C,D. Same as A and B, but with the TGS2620 sensors, which have a faster response time.
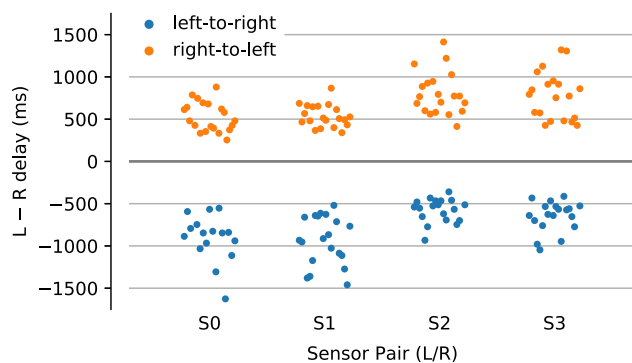

Figure 6. Relative delays between left and right channels encode the direction of travel. Shown here are the delays between the first event on the left channel and the first event on the right channel over 40 trial runs, color-coded by stimulus direction (20 trials with a left-to-right puff and 20 with a right-to-left puff). Three outliers with a delay greater than 2 s are not shown on this graph.

We find that bout onset information lends itself well to event-based encoding and processing. In the past decade, event-based sensors have garnered interest, because they are efficient in bandwidth (transmitting only changes rather than redundant frames) and make certain tasks simpler. While electronic olfaction is still low-bandwidth and low-dimensional compared to vision, this may change as sensor technology improves. Inferring stereo delays from event timing is less computationally expensive than, for instance, from the cross-correlogram of the two channels.

In our experiment, the timing of bout onset events is enough to estimate the direction of a puff of odorant, just like bout frequency was already known to contain information about the distance to the source.[2] Future research should confirm how well that event-based approach translates to real-world conditions, and assess to which extent event timing is sufficient to navigate toward an odor source with more chaotic plumes and lower odorant concentrations.

For instance, the ability of the system to resolve successive bouts at short intervals should be explored systematically.

From the data in Figure 5, we estimate that we can separate successive bouts down to an interval of about 1 to 3 s, but this would have to be quantified in conjunction with ground truth data about the plume structure.

Finally, while we have not quantified the effect of bit depth on the stereo detection task presented here (which uses relatively high concentrations), our system's ability to resolve very low-amplitude fluctuations may also be advantageous when applied to low-concentration plumes.

■ CONCLUSION

Our work demonstrates how a relatively simple and lightweight setup using MOX sensors can extract onset times and separate successive bouts at intervals much shorter than the sensor's recovery time. Increased temporal resolution renders metal oxide sensors more useful in extracting data from turbulent plumes, in particular, when the temporal structure of gas concentration fluctuations is of concern, rather than absolute concentration values.

This highlights their potential for odor-guided navigation in embedded systems such as weight-constrained aerial vehicles.[13] In ground-based robots, the proposed method could remove the need for a separate anemometer to estimate odor source direction.

While the present work focused on temporal resolution, future research should assess whether particular odorants and mixtures of odorants can be reliably identified using the event-based approach. This would constitute a purely event-based system for the simultaneous identification and localization of gas sources.

■ ASSOCIATED CONTENT

Ⓢ🄸 Supporting Information

The Supporting Information is available free of charge at https://pubs.acs.org/doi/10.1021/acssensors.0c02006.

Impact of ADC resolution on the acquisition of low-amplitude signals (PDF)

■ AUTHOR INFORMATION

Corresponding Author

　Damien Drix − *Biocomputation group, Department of Computer Science, University of Hertfordshire, Hatfield AL10 9AB, United Kingdom;* ⬤ orcid.org/0000-0003-4107-5693; Email: d.drix@herts.ac.uk

Author

　Michael Schmuker − *Biocomputation group, Department of Computer Science, University of Hertfordshire, Hatfield AL10 9AB, United Kingdom*

Complete contact information is available at:
https://pubs.acs.org/10.1021/acssensors.0c02006

Notes

The authors declare no competing financial interest.

■ REFERENCES

(1) Mylne, K. R.; Mason, P. J. Concentration fluctuation measurements in a dispersing plume at a range of up to 1000 m. *Q. J. R. Meteorol. Soc.* **1991**, *117*, 177−206.

(2) Schmuker, M.; Bahr, V.; Huerta, R. Exploiting plume structure to decode gas source distance using metal-oxide gas sensors. *Sens. Actuators, B* **2016**, *235*, 636−646.

(3) Pashami, S.; Lilienthal, A. J.; Trincavelli, M. Detecting changes of a distant gas source with an array of MOX gas sensors. *Sensors* **2012**, *12*, 16404−16419.

(4) Korotcenkov, G. The role of morphology and crystallographic structure of metal oxides in response of conductometric-type gas sensors. *Mater. Sci. Eng., R* **2008**, *61*, 1−39.

(5) Gonzalez, J.; Monroy, J. G.; Garcia, F.; Blanco, J. L. The Multi-Chamber Electronic Nose (MCE-nose); 2011 IEEE International Conference on Mechatronics; 2011; pp 1−6. DOI: 10.1109/ICMECH.2011.5971193.

(6) Vergara, A.; Benkstein, K. D.; Montgomery, C. B.; Semancik, S. Demonstration of Fast and Accurate Discrimination and Quantification of Chemically Similar Species Utilizing a Single Cross-Selective Chemiresistor. *Anal. Chem.* **2014**, *86*, 6753−6757.

(7) Arshak, K.; Lyons, G.; Cavanagh, L.; Clifford, S. Front-end signal conditioning used for resistance-based sensors in electronic nose systems: a review. *Sens. Rev.* **2003**, *23*, 230−241.

(8) Martinez, D.; Burgués, J.; Marco, S. Fast Measurements with MOX Sensors: A Least-Squares Approach to Blind Deconvolution. *Sensors* **2019**, *19*, 4029.

(9) Burgués, J.; Valdez, L. F.; Marco, S. High-bandwidth e-nose for rapid tracking of turbulent plumes; 2019 IEEE International Symposium on Olfaction and Electronic Nose (ISOEN); 2019. DOI: 10.1109/ISOEN.2019.8823158.

(10) Vasyutynskyy, V.; Kabitzsch, K. Towards Comparison of Deadband Sampling Types; 2007 IEEE International Symposium on Industrial Electronics; 2007; pp 2899−2904. DOI: 10.1109/ISIE.2007.4375074.

(11) Miskowicz, M. Send-On-Delta Concept: An Event-Based Data Reporting Strategy. *Sensors* **2006**, *6*, 49−63.

(12) Lichtsteiner, P.; Posch, C.; Delbruck, T. A. 128 × 128 120 dB 15 us Latency Asynchronous Temporal Contrast Vision Sensor. *IEEE J. Solid-State Circuits* **2008**, *43*, 566−576.

(13) Burgués, J.; Hernández, V.; Lilienthal, A.; Marco, S. Smelling Nano Aerial Vehicle for Gas Source Localization and Mapping. *Sensors* **2019**, *19*, 478.